
Fine-tuning can cripple your foundation model; preserving features may be the solution

Jishnu Mukhoti¹, Yarin Gal¹, Philip H. S. Torr¹, Puneet K. Dokania^{1,2}
University of Oxford¹ & Five AI Limited²

Abstract

Pre-trained foundation models, owing primarily to their enormous capacity and exposure to vast amount of training data scraped from the internet, enjoy the advantage of storing knowledge about plenty of real-world concepts. Such models are typically fine-tuned on downstream datasets to produce remarkable state-of-the-art performances. While various fine-tuning methods have been devised and are shown to be highly effective, we observe that a fine-tuned model’s ability to recognize concepts on tasks *different* from the downstream one is reduced significantly compared to its pre-trained counterpart. This is clearly undesirable as a huge amount of time and money went into learning those very concepts in the first place. We call this undesirable phenomenon “concept forgetting” and via experiments show that most end-to-end fine-tuning approaches suffer heavily from this side effect. To this end, we also propose a rather simple fix to this problem by designing a method called LDIFS (short for ℓ_2 distance in feature space) that simply preserves the features of the original foundation model during fine-tuning. We show that LDIFS significantly reduces concept forgetting without having noticeable impact on the downstream task performance.

1 Introduction

Foundation models like CLIP [26], ALIGN [12] and CoCa [34] are trained using self-supervised methods on hundreds of millions or even billions of samples scraped from the internet. This massive, compute intensive pre-training makes such models a knowledge store on a vast number of real-world concepts, enabling them to easily transfer to a wide variety of downstream tasks and applications. Indeed, this ability to recognize real-world concepts and thereby transfer to downstream tasks is the primary advantage of such models and is the very reason behind their name [1].

While a foundation model can often achieve an impressive performance on a downstream task without even requiring a single training sample from the task itself [26], in order to maximise performance, it conventionally requires some form of fine-tuning on the task at hand. There are multiple types of fine-tuning methods like linear probing [26], prompt-tuning [38, 37], adapters [5, 35], weight-space interpolation [32, 9] and full end-to-end fine-tuning [26, 17, 7, 33]. Among these types, full end-to-end fine-tuning is generally known to produce the best performance on downstream tasks.

It is worth noting here that the pre-training dataset of a foundation model, owing to its massive scale, contains information on several thousands of real-world concepts. Hence, it is highly likely that the downstream dataset for fine-tuning the model can only contain but a minuscule number of concepts compared to its pre-training set. A natural question that arises then is: *How does end-to-end fine-tuning of a foundation model affect the vast knowledge it acquired through its pre-training?* In this work, this is precisely what we aim to answer.

Through a thorough study of popular end-to-end fine-tuning methods, we observe that for most of them, the fine-tuned model significantly loses its ability to recognize real-world concepts outside the

downstream task, a phenomenon which we call *concept forgetting*. This is a highly undesirable effect as there can be many real-life cases where we would want the foundation model’s vast knowledge on concepts to be preserved over fine-tuning. For instance, a foundation model might not have pre-trained knowledge on certain domains. Specific examples of this include ChatGPT [23] not knowing about events after September 2021 or CLIP under-performing on satellite image classification or lymph node tumor detection [26]. To then update the model with new knowledge, training from scratch on a combined dataset of new and old data is infeasible owing to the enormous cost involved in terms of time, resources and money. Thus, devising methods which update the foundation model without making it forget pre-trained concepts is an important and challenging task. Moreover, it is also hard to say what other properties of a pre-trained model (for example, transferability, generalization, and robustness to name a few) a fine-tuned model would lose due to concept forgetting.

Although conventional end-to-end fine-tuning methods generally suffer from concept forgetting, we find that there can be a relatively simple fix to this problem. In particular, we observe that if a fine-tuning method ensures that the fine-tuned model lies in the vicinity of the original foundation model, it can significantly reduce concept forgetting. While the vicinity of the original model can be defined in terms of distance in the parameter space, as seen in the case of the L2SP regularizer [33], we find that it is much more effective to define it in terms of distance in the model’s feature space which captures its true input-output behaviour. This leads us to propose a new regularizer, **LDIFS** (ℓ_2 **distance in Feature Space**), which minimizes the distance between the features of the original model and those obtained from the model being fine-tuned. We also observe that simply preserving the last-layer features is not effective in reducing concept forgetting, therefore, motivated by [36], we preserve features extracted from different internal representations. We find that this simple method of preserving the original model’s features while fine-tuning on a downstream task, can significantly alleviate the problem of concept forgetting in the fine-tuned model, without affecting its performance on the downstream task. To summarize, our contributions in this work are:

1. **Investigate concept forgetting.** We perform a thorough evaluation, benchmarking 6 existing end-to-end fine-tuning methods on 9 different downstream tasks and find that concept forgetting, as a phenomenon, exists in all of them.
2. **Analyze different end-to-end fine-tuning methods.** We find that the level of concept forgetting is very different for different fine-tuning methods. Particularly the L2SP [33] regularizer consistently outperforms others in lowering concept forgetting and we analyze as to why this is the case.
3. **Propose a new regularizer for end-to-end fine-tuning.** Analyzing L2SP helps us propose a simple regularizer (LDIFS) which minimizes feature space distance while fine-tuning.
4. **A nudge towards continual fine-tuning.** Finally, as a natural extension of the evaluation setting we look at a sequence of 2 fine-tuning tasks instead of 1 and find a desirable performance from LDIFS compared to other fine-tuning methods even in this setting.

2 A brief note on fine-tuning

Here we provide a description of CLIP [26] as our foundation model of choice and briefly discuss existing state-of-the-art fine-tuning methods before discussing their impact on the knowledge of a pre-trained foundation model.

CLIP, a brief overview Broadly speaking, a CLIP model has two components: **i)** the vision or image encoder $f_{\theta_v} : \mathbb{R}^{C,H,W} \rightarrow \mathbb{R}^D$, and **ii)** the text encoder $f_{\theta_t} : \mathbb{R}^L \rightarrow \mathbb{R}^{D^1}$. CLIP is pre-trained on 400 million pairs of images and corresponding text descriptions scraped from the internet. For pre-training, it uses a contrastive loss to maximize cosine similarity between the correct (image, text) pairs and minimize the same for the incorrect ones. Due to its large-scale self-supervised pre-training, CLIP exhibits impressive performance on several downstream tasks, often without requiring a single training sample from the task itself. However, in order to maximise performance on a specific downstream task, the pre-trained CLIP model is conventionally fine-tuned further on the task itself. Below we provide a brief description of such popular fine-tuning methods.

¹Note, the vision encoder first extracts D_v dimensional image features and then projects them to a D dimensional space via a linear embedder $\mathbf{w}_v : \mathbb{R}^{D_v} \rightarrow \mathbb{R}^D$. Similarly for the text encoder.

Zero-shot (ZS) In image classification, given an input image \mathbf{x} and a set of K class names $\{\mathbf{c}_i\}_{i=1}^K$ as the natural language text, the D -dimensional text encoding for each class name $\psi(\mathbf{c}_i) = f_{\theta_t}(\mathbf{c}_i)$ ² and image $\phi(\mathbf{x}) = f_{\theta_v}(\mathbf{x})$ is first obtained. Text encodings are then used as the parameters of a K -class linear classification problem, and the inference is performed simply as $\arg \max_i \psi(\mathbf{c}_i)^\top \phi(\mathbf{x})$. This is known as the zero-shot (ZS) prediction and CLIP’s best model has been shown to have competitive ZS accuracies with a fully supervised ResNet-101 on ImageNet [26].

Linear Probe (LP) In this case, an additional linear layer $\mathbf{w} \in \mathbb{R}^{D \times K}$ is appended on top of the image encoder f_{θ_v} and the weights of this linear layer are trained by solving a standard logistic regression problem (scikit-learn’s `LogisticRegression` module [25] can be used for the same). The linear layer \mathbf{w} is normally initialized using the text representations $\{\psi(\mathbf{c}_i)\}_{i=1}^K$, known as *ZS initialization*. It is trivial to note that in the absence of any training, LP boils down to ZS.

End-to-end fine-tuning While a pre-trained CLIP encoder can obtain impressive ZS and LP accuracies on several tasks, in order to maximize performance on a specific downstream task, the general rule of thumb is to initialize a model from the weights of the pre-trained encoder and then fine-tune the model end-to-end on the downstream task. Here we list some of the most popular end-to-end fine-tuning methods which we study in this work. We provide a more detailed discussion on the different types of fine-tuning methods in §6.

1. **ZS-init-CE** [26]: This is the classic end-to-end fine-tuning method where, similar to the LP, a ZS initialized linear head $\mathbf{w} : \mathbb{R}^D \rightarrow \mathbb{R}^K$ is appended to the image encoder f_{θ_v} . However, differently from the LP, parameters of the entire model $\theta = \{\theta_v, \mathbf{w}\}$ (including the image encoder parameters) are fine-tuned using a cross-entropy loss \mathcal{L}_{CE} .
2. **LP-init-CE (LP-FT)** [17]: This is similar to ZS-init-CE but instead of initializing the appended linear head via ZS, it is initialized by performing linear probing on the downstream task first. Once the linear head is initialized, the entire model is end-to-end fine-tuned using \mathcal{L}_{CE} .
3. **ZS-init-L2SP** [33]: In addition to the cross-entropy loss \mathcal{L}_{CE} used in [26], this method uses an additional regularizer to minimize the ℓ_2 distance between the pre-trained and fine-tuned *image encoder weights*, thereby tries to keep the fine-tuned model weights close to the pre-trained ones. Let the pre-trained image encoder weights be $\theta_{v(0)}$ and the encoder weights at time step t during fine-tuning be $\theta_{v(t)}$. Then, the fine-tuning loss in this case becomes

$$\mathcal{L}_{\text{L2SP}} = \mathcal{L}_{\text{CE}} + \lambda_{\text{L2SP}} \|\theta_{v(t)} - \theta_{v(0)}\|_2^2. \quad (1)$$

Note that the ℓ_2 distance is only computed between the weights of the pre-trained and fine-tuned image encoders.

4. **LP-init-L2SP**: This is similar to ZS-init-L2SP but the linear head \mathbf{w} is initialized by performing linear probing on the downstream dataset first. The loss for end-to-end fine-tuning then is the same as in Equation (1)³.
5. **FLYP** [7]: The Fine-tune Like You Pre-train or FLYP baseline fine-tunes both the image and the text encoders of CLIP and uses contrastive loss $\mathcal{L}_{\text{cont}}$ instead of cross-entropy \mathcal{L}_{CE} for fine-tuning on the downstream task. The parameters being fine-tuned here are $\theta = \{\theta_v, \theta_t\}$, i.e., both image and text encoders of CLIP.
6. **FLYP-CE** [7]: This is an ablation on FLYP where, instead of using contrastive loss, the fine-tuning is done using cross-entropy loss \mathcal{L}_{CE} , taking the cosine similarities between image and text embeddings as logits. Note that similar to FLYP, in this case as well, both image and text encoders are fine-tuned end-to-end.

3 The crippling effect of end-to-end fine-tuning

The contrastive pre-training dataset of CLIP contains 400 million (image, text) pairs scraped from the internet [26]. Consequently, any downstream task that CLIP is fine-tuned on is highly likely to contain only a minuscule number of concepts compared to what it has already been exposed to during pre-training. To investigate the impact of fine-tuning, here we perform a thorough study benchmarking

²Before computing the text encoding, the natural language class names are often further augmented with an additional prompt like “an image of a {class name}.”

³To the best of our knowledge, LP-init-L2SP, as a baseline, has not been evaluated or benchmarked prior to this work.

6 fine-tuning methods on 9 downstream classification tasks. We find that for most of these methods, while the fine-tuned model attains excellent and improved performance on the downstream task itself, its general ability to recognize concepts outside the task is significantly reduced over the course of fine-tuning. We call this phenomenon *concept forgetting* and find this to be an undesirable effect of most fine-tuning methods. To explore this in more detail, in the remainder of the section, we first discuss how we quantify concept forgetting, then we propose our benchmarking setup for fine-tuning methods and finally present our observations.

3.1 Quantifying Concept Forgetting

During ZS and LP evaluation of a model (refer §2) the pre-trained image encoder weights θ_v remain frozen and unchanged irrespective of the downstream task at hand. Therefore, ZS and LP performance on a specific downstream task can be a good indicator of the pre-trained model’s encoded knowledge about the task. This is the hypothesis we base our analysis on.

Furthermore, while ZS accuracy is based on how well the text encoder representations can separate task-specific categories in the image encoder’s feature space, LP performance is indicative of whether image encoder representations are linearly separable. This distinction is important as changing the weights of the image encoder θ_v during end-to-end fine-tuning can lead to a situation where its representations are no longer well-aligned with the text encoder. Even so, for a given task, if the image encoder representations are linearly separable, it indicates that the model is still able to recognize concepts involved in the downstream task, thereby indicative of the pre-trained model’s encoded knowledge on the downstream task.

Therefore, in order to quantify concept forgetting over fine-tuning, we simply measure the difference in both ZS and LP accuracy between the pre-trained and fine-tuned image encoders. To formalize this, let $f_{\theta_{v(0)}}$ and f_{θ_v} be the pre-trained and fine-tuned image encoders respectively, and let \mathcal{D}_{ft} represent the task on which we fine-tune $\theta_{v(0)}$. Furthermore, let $\mathcal{A}_{ZS}(f_{\theta_v}, \mathcal{D})$ and $\mathcal{A}_{LP}(f_{\theta_v}, \mathcal{D})$ represent the ZS and LP accuracy of image encoder f_{θ_v} on task \mathcal{D} . Then, we can define concept forgetting on task \mathcal{D} as the change in LP (or ZS) accuracy on task \mathcal{D} between pre-trained and fine-tuned models: $\Delta_{LP}(\mathcal{D}, f_{\theta_v}, f_{\theta_{v(0)}})$ (or in short, Δ_{LP}) as:

$$\Delta_{LP}(\mathcal{D}, f_{\theta_v}, f_{\theta_{v(0)}}) = \mathcal{A}_{LP}(f_{\theta_v}, \mathcal{D}) - \mathcal{A}_{LP}(f_{\theta_{v(0)}}, \mathcal{D}) \tag{2}$$

We can define $\Delta_{ZS}(\mathcal{D}, f_{\theta_v}, f_{\theta_{v(0)}})$ in a similar manner. Clearly, as the image encoder θ_v is obtained after fine-tuning on \mathcal{D}_{ft} , we can expect $\Delta_{LP}(\mathcal{D}_{ft}, f_{\theta_v}, f_{\theta_{v(0)}})$ and $\Delta_{ZS}(\mathcal{D}_{ft}, f_{\theta_v}, f_{\theta_{v(0)}})$ to increase over the course of fine-tuning. However, the more interesting case is to capture concept forgetting of the model over tasks other than the fine-tuning task itself, i.e., $\Delta_{ZS}(\mathcal{D}, f_{\theta_v}, f_{\theta_{v(0)}})$ and $\Delta_{LP}(\mathcal{D}, f_{\theta_v}, f_{\theta_{v(0)}})$ when $\mathcal{D} \neq \mathcal{D}_{ft}$. A negative value for these metrics indicates concept forgetting and zero indicates knowledge accumulation. However, a positive value indicates knowledge gain on the task under inspection.

Catastrophic forgetting vs concept forgetting Catastrophic forgetting [21, 13, 14] is a well-known phenomenon which signifies how, when a model is trained on a new task, its performance on the previously task drops catastrophically. For example, a model trained on ImageNet is when further trained on say CIFAR100 almost completely loses its performance on ImageNet. Though *concept forgetting* mentioned in this work is very similar to catastrophic forgetting and we do not claim much conceptual novelty here, there still are subtle differences that we believe requires a distinction between the two. The major difference being the fact that in the pre-foundation model era it was known exactly on which task or dataset a model was trained (for example, ImageNet in the example above) and therefore, it was possible to roughly quantify the degree of damage the model had once it was fine-tuned on a new downstream task. However, in the case of foundation models, it is not possible to quantify exactly what the model knows as the model was pre-trained on millions (or even billions) of examples, therefore, it is not possible to quantify exactly what the fine-tuned model forgot and the catastrophe therein. Hence, it is necessary to devise poking mechanisms similar to the ones presented in this work using ZS and LP, to quantify the effect (forgetting) of fine-tuning on a small but useful domain of concepts (represented by the dataset \mathcal{D} used to quantify Δ_{LP} or similar metrics).

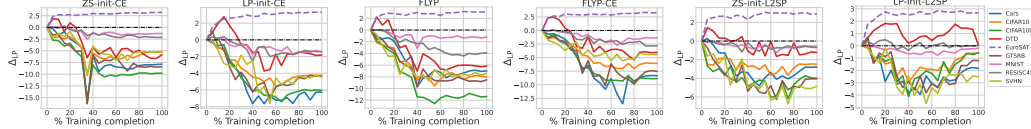


Figure 1: **Test set Δ_{LP} for models fine-tuned on EuroSAT using different fine-tuning methods.** While EuroSAT Δ_{LP} rises, Δ_{LP} on all other datasets is almost always negative throughout the fine-tuning with a sole exception of DTD when fine-tuned using LP-init-L2SP. See §3.2 for details.

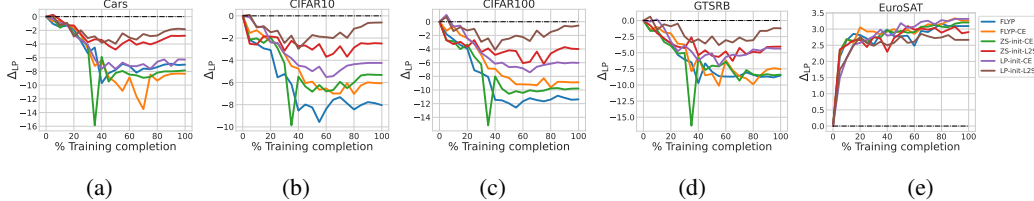


Figure 2: **Test set Δ_{LP} evaluated on different datasets for models fine-tuned on EuroSAT via various fine-tuning methods.** The L2SP baselines (particularly LP-init-L2SP) have the lowest negative Δ_{LP} on datasets other than EuroSAT.

3.2 Benchmarking concept forgetting

To quantify concept forgetting, here we use CLIP [26] ViT-B/32 pre-trained on the OpenAI dataset and released in the OpenCLIP repository [11] and measure its ZS and LP performance over fine-tuning on 9 different image classification downstream tasks with a high variability in their semantic concepts. These datasets, along with their respective train/test splits are:

1. *Stanford Cars* [15] containing 16185 images of 196 classes of cars with a train/test split of 8144 and 8041 images respectively,
2. *CIFAR-10/100 (C10/100)* [16] containing 60000 images of vehicles, flora and fauna, divided into 10/100 classes with the train/test split for both C10 and C100 having 50000 and 10000 images respectively,
3. *DTD* [4] containing 3760 images of 47 classes of textures found in the wild with 1880 images each in the train and test sets,
4. *EuroSAT* [8] containing 25000 samples with 10 categories of satellite images of landscapes and 19600/5400 training/test images respectively,
5. *GTSRB* [29] containing 39270 images of 43 classes of German traffic signs with 26640 training images and 12630 test images,
6. *MNIST* [18] containing 60000 training images and 10000 test images of 10 digits from 0 to 9 in grayscale,
7. *RESISC45* [3] containing 25200 samples with 45 classes of various remote sensing image scenes with the train/test split having 18900 and 6300 images respectively,
8. *SVHN* [22] containing a total of 99289 colour images of street view house numbers, each image being categorized into one of 10 digits with 73257 training samples and 26032 test samples.

Finally, for this study, we use the 6 end-to-end fine-tuning methods discussed in §2. The training details can be found in Appendix A.

Fine-tuning causes concept forgetting. In Figure 1, we present the Δ_{LP} for models fine-tuned on EuroSAT using the 6 fine-tuning methods discussed in §2. Across all fine-tuning methods, we observe that *while performance on EuroSAT test set increases and Δ_{LP} is positive (also see Figure 2e), performance on all 8 other downstream datasets decreases and Δ_{LP} for all of them is negative.* This indicates, that *all 6 fine-tuning methods suffer from concept forgetting.* However, the only exception to this observation is when we evaluate on DTD and the model is fine-tuned using LP-init-L2SP. We observe Δ_{LP} to be mostly positive before it goes to zero at the end of fine-tuning. This is an interesting case as it indicates that LP-init-L2SP fine-tuning on EuroSAT might actually be helping increase knowledge about DTD before the fine-tuning becomes too specific to EuroSAT. This may

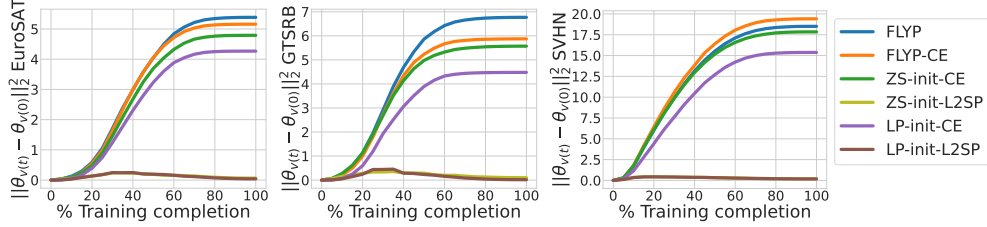


Figure 3: ℓ_2 distance in the parameter space $\|\theta_{v(t)} - \theta_{v(0)}\|_2^2$ of the image encoder over the course of fine-tuning. Except L2SP baselines, all other fine-tuning methods diverge away from their pre-trained counterparts.

be an example of positive forward transfer [19, 2] perhaps due to the textures present in EuroSAT. Exploring why such knowledge accumulation happens is an interesting avenue for further research.

Next, we compare between these fine-tuning methods by showing Δ_{LP} for these methods for different downstream datasets in Figure 2. Interestingly, *LP-init-L2SP consistently outperforms others in preserving the fine-tuned model’s original performance across multiple downstream tasks*, as is observable from its low negative Δ_{LP} compared to other baselines. While it suffers an initial dip in performance in the early stages of fine-tuning, in the later stages, LP-init-L2SP regains the accuracy, often ending up with a near zero Δ_{LP} . Its impressive performance however, does seem to come at the cost of a relatively lower positive Δ_{LP} on the fine-tuning task, i.e., EuroSAT, itself. We provide such plots on other datasets in Appendix C. In what follows, we first investigate LP-init-L2SP further to gain some insights on why it preserves concepts better than the other baselines, and then use those insights to propose a new fine-tuning method that significantly outperforms all the baselines.

4 Can preserving features help?

The L2SP regularizer (Equation (1)) enforces the model $f_{\theta_{v(t)}}$ at time-step t of the fine-tuning to be in the vicinity of the pre-trained model $f_{\theta_{v(0)}}$ by minimizing the ℓ_2 distance between the two in the parameter space. As is evident from §3, this simple regularizer has a promising impact on model’s ability to avoid concept forgetting. To understand how correlated the parameter space distance $\|\theta_{v(t)} - \theta_{v(0)}\|_2^2$ is to concept forgetting, in Figure 3, we show how ℓ_2 distance changes as we fine-tune different datasets (EuroSAT, GTSRB and SVHN) using all the discussed fine-tuning methods. The observation is crystal clear. *Relatively speaking, all the fine-tuning methods except the two L2SP baselines (ZS-init-L2SP and LP-init-L2SP) cause the parameters of the fine-tuned model to significantly move away from its pre-trained counterpart.* For the L2SP baselines, $\|\theta_{v(t)} - \theta_{v(0)}\|_2^2$ first increases and then falls back down indicating that the model first diverges slightly and then gets closer again to the pre-trained model in the parameter space.

Though keeping the fine-tuned model in the vicinity of the pre-trained one during fine-tuning did show highly promising effect in preserving concepts, however, vicinity in the parameter space need not necessarily capture the true input-output behaviour of the pre-trained model. For example, it is trivial to construct two different sets of model parameters (far in ℓ_2 distance) outputting similar values in a specific domain. Additionally, regularizing in the parameter space might not keep the fine-tuned model in the *desired* vicinity that captures the knowledge of the pre-trained model. Therefore, we conjecture that the vicinal distance in the feature space might be a better indicative of how effectively models can preserve concepts as, in the end, internal representation space is where models encode patterns. Thus, in Figure 4, we inspect the ℓ_2 distance in the feature space over the course of fine-tuning using the following distance function:

$$d(\theta_{v(t)}, \theta_{v(0)}, \mathcal{D}) = \frac{1}{N} \sum_{i=1}^N \|\Phi_{\theta_{v(t)}}(\mathbf{x}_i) - \Phi_{\theta_{v(0)}}(\mathbf{x}_i)\|_2^2, \quad (3)$$

where, $\Phi_{\theta_{v(t)}}(\mathbf{x}_i)$ represents the features of the model with parameters $\theta_{v(t)}$ at time t for a given sample \mathbf{x}_i , and N is the number of samples in the dataset. Note that the feature vector $\Phi_{\theta_{v(t)}}(\mathbf{x}_i)$ is obtained by concatenating various internal representations (not just the last layer features) of the network architecture, similar to the perceptual features presented in [36]. Exact details as to how

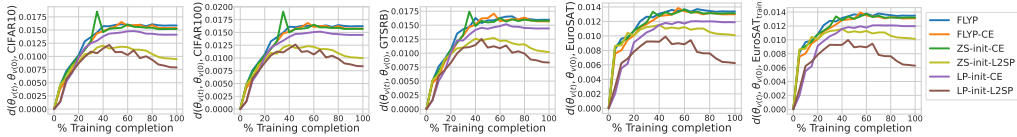


Figure 4: ℓ_2 distance in feature space $d(\theta_{v(t)}, \theta_{v(0)}, \mathcal{D})$ between image encoders computed over the course of fine-tuning on EuroSAT.

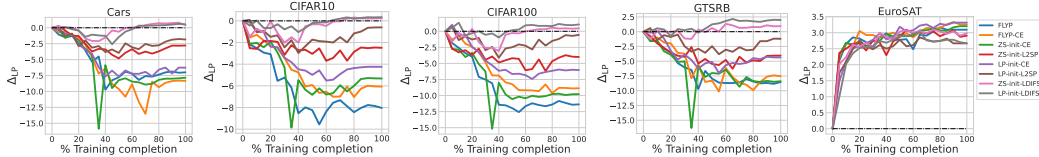


Figure 5: Test set Δ_{LP} evaluated on different datasets for models fine-tuned on EuroSAT. LDIFS (Our) baselines (both ZS-init and LP-init) provides the best results in terms of avoiding concept forgetting without affecting downstream performance on EuroSAT.

we compute the concatenated feature vector for a ViT-B/32 model is mentioned in Appendix B, and similar plots for other datasets is shown in Appendix C.

A strong correlation between concept forgetting and feature-space distance. Similar to our observations in Figure 3 (parameter space), we note that except L2SP, all other fine-tuning methods suffering significantly from concept forgetting cause the fine-tuned model to move away from the pre-trained model in terms of feature-space distance as well (Equation (3)). In case of ZS-init-L2SP and LP-init-L2SP, while initially diverging, the fine-tuned models recover their pre-trained behaviour to a certain extent in the later stages of fine-tuning. It is important to note that this observation is consistent for the fine-tuning training and test sets as well as for all other datasets.

Therefore, based on the empirical results shown in Figure 2 and Figure 4 we conclude that the fine-tuning methods which cause the model to significantly diverge away from the pre-trained model either in parameter space or in feature space suffer more from concept forgetting. Above observations combined with our conjecture lead to a natural extension of the existing fine-tuning methods where $d(\theta_{v(t)}, \theta_{v(0)}, \mathcal{D})$ (distance in the feature space) is being used as the regularizer. We call this regularizer **LDIFS: ℓ_2 distance in Feature Space**, the complete fine-tuning objective then becomes:

$$\mathcal{L}_{LDIFS} = \mathcal{L}_{CE} + \lambda_{LDIFS} \cdot d(\theta_{v(t)}, \theta_{v(0)}, \mathcal{D}_{\text{train}}) \quad (4)$$

where $\mathcal{D}_{\text{train}}$ is the training set and λ_{LDIFS} is the regularization coefficient. Note that similar to L2SP, we can initialize the linear head with both zero-shot weights or linear probed weights leading to two variants: ZS-init-LDIFS and LP-init-LDIFS.

LP-init-LDIFS minimizes concept forgetting with competitive fine-tuned performance. We evaluate ZS-init-LDIFS and LP-init-LDIFS on the same setting discussed in §3 and present the Δ_{LP} over fine-tuning in Figure 5 (additional results presented in Appendix C). Correspondingly, in Table 1, we report the Δ_{ZS} , Δ_{LP} (see Equation (2)) and the \mathcal{A}_{LP} accuracy of the fully fine-tuned models for EuroSAT, GTSRB and SVHN. The full set of results on all 9 datasets is presented in Table 3 of the Appendix. Our observations are as follows.

1. From Figure 5, we note that both ZS-init-LDIFS and LP-init-LDIFS are competitive with all fine-tuning baselines in terms of \mathcal{A}_{LP} accuracy on the fine-tuning task itself.
2. **Both the LDIFS baselines, in particular LP-init-LDIFS, significantly minimize concept forgetting over the course of fine-tuning.** This is evident from Figure 5 which show their noticeably lower negative Δ_{LP} on other downstream tasks over the course of fine-tuning. It is also apparent from their consistently high Δ_{ZS} and Δ_{LP} scores in Table 1 and Table 3. As a specific example, on EuroSAT, Δ_{LP} is negative on all 8 other classification tasks for all baselines except LP-init-L2SP, for which Δ_{LP} is negative on 6 out of the 8 tasks. In contrast, ZS-init-LDIFS has negative Δ_{LP} on merely 2 out of the 8 tasks and LP-init-LDIFS has no negative Δ_{LP} at all. This indicates a significantly minimized level of concept forgetting. Similar observations can be made for models fine-tuned on other datasets.

Dataset	Final	Fine-tuning baselines																										
		FLYP			FLYP-CE			ZS-init-CE			LP-init-CE (LP-FT)			ZS-init-L2SP			LP-init-L2SP			ZS-init-LDIFS (Ours)			LP-init-LDIFS (Ours)					
		$\Delta_{ZS}(T)$	$\Delta_{LP}(T)$	$\mathcal{A}_{LP}(T)$	$\Delta_{ZS}(T)$	$\Delta_{LP}(T)$	$\mathcal{A}_{LP}(T)$	$\Delta_{ZS}(T)$	$\Delta_{LP}(T)$	$\mathcal{A}_{LP}(T)$	$\Delta_{ZS}(T)$	$\Delta_{LP}(T)$	$\mathcal{A}_{LP}(T)$	$\Delta_{ZS}(T)$	$\Delta_{LP}(T)$	$\mathcal{A}_{LP}(T)$	$\Delta_{ZS}(T)$	$\Delta_{LP}(T)$	$\mathcal{A}_{LP}(T)$	$\Delta_{ZS}(T)$	$\Delta_{LP}(T)$	$\mathcal{A}_{LP}(T)$	$\Delta_{ZS}(T)$	$\Delta_{LP}(T)$	$\mathcal{A}_{LP}(T)$	$\Delta_{ZS}(T)$	$\Delta_{LP}(T)$	$\mathcal{A}_{LP}(T)$
EuroSAT	Cas	-18.44	-7.0	73.8	-14.04	-8.34	72.45	-12.34	-7.85	72.95	-13.0	-6.27	74.53	-4.89	-2.79	78.01	-3.95	-1.84	78.97	-1.37	0.42	81.22	-1.08	0.53	81.33	-1.84	0.54	80.25
	CFAR10	-20.75	-9.04	86.86	-17.0	-6.07	88.84	-17.99	-5.32	89.59	-12.77	-4.24	90.08	-5.87	-2.49	92.41	-1.59	-0.6	94.31	-0.53	0.28	95.13	0.09	0.54	90.89	0.54	89.25	
	CFAR100	-30.66	-11.57	68.26	-23.68	-8.87	70.76	-24.64	-9.78	69.85	-17.79	-6.03	73.59	-6.43	-4.0	75.62	-0.83	-0.56	79.08	1.23	0.46	80.09	2.27	1.06	80.7	2.27	1.06	80.7
	FTD	-10.85	-1.2	97.45	-7.5	-4.04	98.03	-7.13	-3.85	98.33	-6.12	-1.81	99.27	-2.93	-1.22	99.85	-1.17	0.05	99.23	1.03	1.19	97.27	1.12	2.66	98.74	1.12	2.66	
	GTSRB	-9.49	-8.53	78.14	-5.78	-7.54	79.16	-6.39	-8.39	78.35	-4.29	-4.35	82.31	-1.27	-4.05	82.6	-0.58	-1.2	85.53	4.66	0.94	87.67	4.51	1.08	88.6	4.51	1.08	
	MNIST	-6.85	-1.2	97.45	-6.92	-1.35	97.32	-7.76	-1.32	97.29	-5.24	-1.48	97.14	3.21	-0.54	98.16	0.04	-0.2	98.44	5.54	-0.07	98.57	2.52	0.13	98.74	2.52	0.13	
	SVHN	-40.95	-3.89	87.97	-28.6	-2.83	89.05	-28.44	-2.16	89.7	-16.65	-1.4	90.48	-8.29	-0.7	91.16	-0.46	0.05	91.3	-4.08	0.9	93.79	0.27	0.27	92.67	0.9	0.79	92.67
SVHN	-18.42	-7.38	88.69	-12.7	-4.44	91.17	-14.24	-3.12	90.32	-10.42	-1.45	91.13	0.07	-4.86	90.56	1.99	-2.51	93.68	0.08	2.5	97.92	0.67	3.03	98.59	0.67	3.03		
GTSRB	Cas	-32.45	-13.23	67.37	-19.66	-9.45	71.36	-20.69	-8.39	72.42	-18.07	-7.61	73.2	-5.77	-2.75	78.05	-1.24	-0.25	80.55	-2.66	0.33	80.94	-0.88	1.82	81.11	-0.88	1.82	
	CFAR10	-61.3	-17.99	76.92	-31.36	-8.35	86.57	-41.57	-12.51	82.4	-15.19	-4.71	90.21	-40.89	-11.41	83.51	-1.77	-0.2	94.72	-1.71	-0.38	94.53	-0.14	0.0	94.92	-0.14	0.0	
	CFAR100	-55.13	-24.28	55.36	-30.12	-12.83	69.83	-42.57	-19.81	59.82	-23.7	-6.2	73.43	-41.4	-17.66	61.97	0.46	0.38	80.01	-2.36	-0.91	78.73	1.81	1.21	80.85	1.81	1.21	
	FTD	-24.68	-14.63	57.45	-10.0	-7.5	64.57	-17.18	-9.2	62.87	-10.74	-3.51	68.83	-6.6	-2.13	69.84	-1.54	1.76	73.72	-2.35	1.65	73.62	-0.32	1.17	73.63	-0.32	1.17	
	EuroSAT	-36.94	-5.0	90.56	-19.21	-2.91	93.03	-21.91	-4.72	90.81	-17.7	-1.11	94.43	-16.5	-3.31	92.22	0.94	0.9	88.54	1.17	-0.43	95.11	2.57	-0.06	95.48	2.57	-0.06	
	MNIST	-6.53	-0.81	97.69	-6.43	-0.25	98.35	-13.95	-0.63	98.02	-1.72	-0.09	98.6	-4.72	-0.39	98.33	3.33	-0.06	98.58	-2.23	0.13	98.8	6.78	0.02	98.66	6.78	0.02	
	SVHN	-46.96	-10.35	81.52	-19.24	-5.44	88.43	-35.92	-8.73	83.14	-18.17	-2.43	89.43	-13.68	-2.89	88.95	0.1	-0.02	91.46	-2.6	-0.48	91.4	0.32	0.11	91.88	0.32	0.11	
SVHN	2.22	18.35	83.82	5.07	16.66	82.25	2.74	16.81	82.08	10.11	18.12	83.65	15.22	16.15	81.75	9.68	7.79	73.39	10.08	8.67	74.17	7.94	5.9	71.45	7.94	5.9		
SVHN	Cas	-39.37	-17.56	63.23	-31.22	-17.22	61.59	-33.06	-18.38	62.43	-30.44	-15.28	65.51	-5.66	-2.92	77.9	-6.63	-2.0	78.8	-6.5	-2.04	78.76	-8.73	-2.89	77.91	-8.73	-2.89	
	CFAR10	-44.46	-13.57	81.34	-30.88	-13.84	81.06	-42.24	-14.41	80.5	-32.49	-11.44	83.49	-21.11	-7.47	87.45	-28.95	-6.06	89.25	-7.25	-2.16	92.75	-6.83	-1.86	93.66	-6.83	-1.86	
	CFAR100	-52.73	-21.64	58.0	-43.38	-22.93	56.72	-46.16	-24.14	55.51	-41.28	-18.07	61.59	-28.52	-11.84	67.8	-30.95	-10.09	69.56	-12.88	-5.78	74.38	-11.03	-2.73	76.9	-11.03	-2.73	
	FTD	-28.51	-19.2	52.87	-20.11	-15.48	56.6	-24.1	-18.09	53.88	-20.48	-13.11	56.97	-13.8	-1.86	71.17	-7.45	-0.9	71.12	-4.47	-0.48	71.76	-1.46	0.21	72.29	-1.46	0.21	
	EuroSAT	-36.17	-4.31	91.22	-25.59	-4.3	91.24	-34.87	-5.7	89.83	-36.09	-6.04	89.5	-19.98	-2.26	93.28	-27.78	-2.56	92.08	-2.61	-0.78	94.30	-1.74	-0.78	94.76	-1.74	-0.78	
	GTSRB	-21.91	0.0	86.68	-10.66	0.95	87.72	-8.27	1.78	88.41	-9.62	4.05	91.57	1.8	5.04	91.7	-0.06	6.03	92.61	5.69	6.03	92.66	6.45	6.23	92.9	6.45	6.23	
	SVHN	-44.29	-9.59	82.59	-34.94	-10.1	81.78	-37.16	-10.0	81.87	-40.17	-8.97	82.9	-8.44	-1.95	89.92	-7.84	-1.65	90.23	-4.56	-1.38	90.49	-5.36	-1.0	90.87	-5.36	-1.0	
SVHN	65.0	31.92	97.44	64.38	31.86	97.4	65.98	31.79	97.3	61.28	31.98	97.5	64.84	31.02	96.5	61.39	31.04	96.54	65.25	31.36	96.97	50.92	31.38	96.95	50.92	31.38		

Table 1: Δ_{ZS} , Δ_{LP} and \mathcal{A}_{LP} for models fully fine-tuned on EuroSAT, GTSRB and SVHN. LP-init-LDIFS outperforms other fine-tuning baselines and even LP-init-L2SP in minimizing concept forgetting, while also outperforming LP-init-L2SP on the fine-tuned task performance.

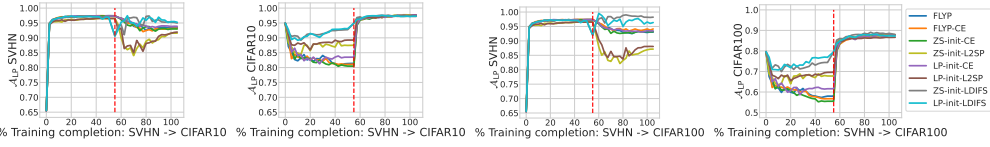


Figure 6: \mathcal{A}_{LP} for different fine-tuning methods for models fine-tuned on the sequence of tasks, i) SVHN \rightarrow CIFAR10 (left 2 plots) and ii) SVHN \rightarrow CIFAR100 (right 2 plots). The vertical red line indicates a switch in the fine-tuning tasks.

3. From Table 1 and Table 3, we also observe that in a lot of the fine-tuning tasks, LP-init-LDIFS results in a positive Δ_{LP} on other tasks, thereby generally achieving a positive forward transfer. The main exception is when the finetuning task \mathcal{D}_{ft} is SVHN, in which case Δ_{LP} is mostly negative on other tasks. This observation also signifies how the ordering of fine-tuning tasks can also impact forward transfer. In fact, when fine-tuning on EuroSAT, LP-init-LDIFS achieves a Δ_{LP} of +3.03 on SVHN, whereas in the reverse scenario, fine-tuning on SVHN leads to a negative Δ_{LP} of -0.78 on EuroSAT.

5 A nudge towards concept accumulation via continual fine-tuning

Our results above indicate that fine-tuning on LP-init-LDIFS can make the foundation model learn new information about a downstream task without forgetting concepts that it had learnt as a result of its pre-training. A natural question that then arises is: *Can we fine-tune on a sequence of downstream tasks without forgetting concepts?* For an ideal fine-tuning method, the final model would attain state-of-the-art performance on all fine-tuned tasks while still maintaining its knowledge on pre-trained concepts. Here, we try to empirically answer this question by training on a sequence of two tasks: a) SVHN \rightarrow CIFAR10 and b) SVHN \rightarrow CIFAR100. This setup is similar to continual learning [2, 27, 19] but for foundation models. Due to their impressive ZS and LP performance on a lot of general downstream tasks, continual fine-tuning of foundation models is relatively unexplored in the literature. Nonetheless, as stated in §1, this is an important problem to investigate from the perspective of updating a foundation model with new knowledge without making it forget previously trained concepts.

In order to quantify concept forgetting on a task \mathcal{D} over a sequence of models $f_{\theta_0}, \dots, f_{\theta_k}$ fine-tuned on the task sequence $\mathcal{D}_1 \rightarrow \mathcal{D}_2 \rightarrow \dots, \mathcal{D}_k$, following intuitions from [2], we extend the Δ_{LP} from Equation (2) as follows:

$$\Delta_{LP}(\mathcal{D}, f_{\theta_k}, \{f_{\theta_0}, f_{\theta_1}, \dots, f_{\theta_{k-1}}\}) = \mathcal{A}_{LP}(f_{\theta_k}, \mathcal{D}) - \max_{i \in \{0, \dots, k-1\}} \mathcal{A}_{LP}(f_{\theta_i}, \mathcal{D}). \quad (5)$$

Δ_{ZS} can also be defined in a similar manner. Note that we find the difference in ZS or LP performance between the final fine-tuned model f_{θ_k} and the model having the maximum ZS or LP performance in the sequence $\{f_{\theta_0}, f_{\theta_1}, \dots, f_{\theta_{k-1}}\}$. It is trivial to see that when fine-tuning on a single task, Equation (5) reduces to Equation (2). In Table 2, we present the Δ_{ZS} , Δ_{LP} and \mathcal{A}_{LP} for the sequence setup for all the baselines.

Clearly, even when the model is trained on a the sequence of two tasks, LDIFS preserves the fine-tuned performance of the first task when the model is fine-tuned on the second one, while other baselines

Dataset	Eval	FLYP			FLYP-CE			Fine-tuning baselines																	
		$\Delta_{ZS}(\uparrow)$	$\Delta_{LP}(\uparrow)$	$A_{LP}(\uparrow)$	$\Delta_{ZS}(\uparrow)$	$\Delta_{LP}(\uparrow)$	$A_{LP}(\uparrow)$	ZS-init-CE			LP-init-CE (LP-FT)			ZS-init-L2SP			LP-init-L2SP			ZS-init-LDIFS (Ours)			LP-init-LDIFS (Ours)		
SVHN \rightarrow CIFAR10	SVHN	52.84	27.98	93.5	53.48	27.68	93.23	57.21	27.48	92.99	43.77	28.52	93.88	51.54	26.11	91.59	40.15	26.44	91.94	56.91	29.36	94.98	58.75	29.68	95.04
	CIFAR10	7.81	2.77	97.68	7.7	2.52	97.42	7.81	2.57	97.48	7.31	2.8	97.73	7.88	2.69	97.63	6.49	2.62	97.53	7.71	2.29	97.2	6.16	2.38	97.3
	CoOp	-57.63	-16.23	64.56	-47.56	-10.07	70.74	-47.11	-9.44	71.37	-40.44	-10.45	70.35	-18.94	-0.06	80.78	-5.52	0.36	81.16	-13.29	0.44	81.23	-4.79	-1.01	79.79
	CIFAR100	-24.27	-0.03	79.61	-4.27	0.06	79.71	-3.24	-0.64	79.01	-2.24	1.59	81.25	6.78	3.86	83.5	7.67	4.72	84.37	2.89	0.82	80.46	3.78	2.25	81.88
	DiT	-19.41	-11.83	60.27	-10.8	-10.06	61.12	-11.26	-9.1	62.87	-12.45	-9.2	62.87	-2.93	0.48	72.71	-3.67	0.8	72.82	-0.98	0.05	72.29	-1.65	1.12	73.19
SVHN \rightarrow SVHN	DiT	-21.36	-0.91	94.63	-20.07	-0.17	95.37	-15.2	-0.35	95.19	-22.02	-0.43	95.11	4.15	-0.13	95.41	-10.28	0.11	95.65	-1.93	0.24	95.78	3.37	0.3	95.83
	DiT	-9.12	-1.78	84.9	-6.33	0.86	87.62	-2.92	0.68	87.31	-4.92	1.68	89.3	4.72	3.14	89.83	4.17	4.15	90.75	7.17	3.24	89.87	7.69	2.95	89.61
	DiT	34.62	-0.04	98.41	28.9	0.15	98.81	36.26	0.11	98.74	7.31	0.33	98.99	28.31	0.22	98.9	13.05	0.13	98.8	2.89	0.2	98.6	-0.55	-0.1	98.56
	DiT	-36.56	-6.03	85.84	-22.29	-4.35	87.52	-20.76	-4.52	87.35	-23.3	-4.33	87.54	-1.31	-0.76	91.13	-2.51	-0.59	91.29	0.46	-0.25	91.62	0.4	0.17	92.65
	DiT	54.08	27.54	93.06	56.19	28.59	94.13	56.72	27.67	93.18	45.18	8.12	93.47	42.11	21.68	87.15	33.62	22.57	88.06	57.84	31.11	87.94	58.61	31.29	96.86
SVHN \rightarrow CIFAR100	CIFAR100	23.18	8.26	87.9	21.64	8.26	87.91	23.78	7.98	87.63	15.63	8.08	87.74	23.66	7.9	87.54	13.47	6.99	86.64	24.37	8.3	87.94	13.56	7.65	87.28
	CoOp	-89.5	-7.77	73.01	-20.4	-8.31	72.5	-22.01	-8.41	72.4	-17.7	-8.36	72.64	-6.89	-8.14	80.08	-1.99	0.27	81.07	-11.19	-0.62	80.18	-4.51	-0.49	80.31
	CIFAR10	-10.04	0.52	95.43	-0.8	0.8	95.7	-2.81	0.92	95.83	0.52	1.12	96.05	2.7	1.03	96.85	3.01	1.84	96.75	-0.05	1.33	96.24	0.61	1.16	96.68
	DiT	-12.18	-9.1	62.98	-12.71	-8.58	63.51	-13.83	-9.36	62.61	-9.89	-8.3	63.78	-5.21	0.0	72.23	-3.19	0.27	72.29	-4.04	-1.54	70.69	-2.55	-0.32	71.76
	DiT	-24.52	-15.2	65.52	-18.85	-4.8	65.06	-20.76	-15.92	65.92	-18.85	0.09	65.63	1.87	-0.13	65.41	-10.09	0.13	65.67	-6.29	-0.07	65.46	-1.28	0.31	65.55
SVHN \rightarrow SVHN	DiT	-6.26	-0.03	86.65	-6.6	1.59	88.36	-5.4	1.31	87.94	2.42	3.44	90.06	4.96	2.79	89.46	4.92	3.62	90.22	2.67	3.43	90.05	5.49	4.33	91.0
	DiT	21.79	0.19	98.84	35.77	0.22	98.88	38.24	0.25	98.88	11.51	0.36	99.02	25.84	0.18	98.86	15.59	0.32	98.92	6.95	0.43	98.83	4.82	0.34	99.0
	DiT	-25.98	-4.84	87.03	-23.4	-4.6	87.27	-20.44	-4.52	87.35	-23.06	-3.35	88.52	-6.05	-0.89	90.98	-4.52	-0.78	91.1	-8.84	-0.94	90.94	-6.24	-0.87	91.0
	DiT	-89.5	-7.77	73.01	-20.4	-8.31	72.5	-22.01	-8.41	72.4	-17.7	-8.36	72.64	-6.89	-8.14	80.08	-1.99	0.27	81.07	-11.19	-0.62	80.18	-4.51	-0.49	80.31
	DiT	-10.04	0.52	95.43	-0.8	0.8	95.7	-2.81	0.92	95.83	0.52	1.12	96.05	2.7	1.03	96.85	3.01	1.84	96.75	-0.05	1.33	96.24	0.61	1.16	96.68

Table 2: Δ_{ZS} , Δ_{LP} and A_{LP} for models fine-tuned on SVHN \rightarrow CIFAR10 and SVHN \rightarrow CIFAR100. LP-init-LDIFS consistently outperforms other baselines even in the sequence setup.

seem to lose out on performance on the first task over the second fine-tuning stage. This is complemented by our observations in Figure 6 where we can see that while all fine-tuning methods other than LDIFS obtain state-of-the-art performance on the second fine-tuning task: CIFAR10/CIFAR100, they generally lose performance on SVHN. This is not the case for LDIFS however, where performance on SVHN is broadly maintained as the models are fine-tuned on the second task: CIFAR-10/100.

6 Related Work

In this section, we provide a brief discussion on the different types of fine-tuning approaches apart from end-to-end fine-tuning which have been applied on foundation models. We also discuss the difference between our regularizer LDIFS and the well-known LPIPS [36] metric.

Types of fine-tuning in foundation models: Apart from end-to-end fine-tuning, there are other types of fine-tuning as well which try to improve on a CLIP model’s zero-shot performance. A popular approach is prompt tuning where, methods like CoOp [38] and CoCoOp [37], instead of hand-crafting prompts for obtaining text encoder representations, learn the prompts specific to the fine-tuning task. Some other works on prompt tuning include TPT [28], which performs prompt tuning at test time and Chain of Thought prompt tuning [6] which emulates the chain of thought in CLIP using multiple prompt steps. Another category of methods uses adapters: CLIP-Adapter [5], Tip-Adapter [35], Prompt Adapter [30], SVL-Adapter [24], which works on the principle of combining pre-trained features with a small non-linear adapter network where the adapter is fine-tuned on the downstream task at hand. Finally, along with end-to-end fine-tuning, there are weight space interpolation methods like Wise-FT [32], PAINT [10], task arithmetic [9] and model soups [31] which look at interpolating between pre-trained and fine-tuned models in the weight space in order to achieve the best of both worlds in terms of downstream task performance as well as robustness to distribution shift. Note that these approaches are orthogonal to full end-to-end fine-tuning and one could of course think of creative ways of combining these methods with fine-tuning approaches.

Relation between LDIFS and LPIPS [36]: Although similar in formulation to LPIPS [36], LDIFS uses the feature space ℓ_2 distance in a completely different manner. While LPIPS uses feature space distance on a *pre-trained, frozen* model to find perceptual similarity between pairs or sets of images, LDIFS instead feature space distance between a pair of pre-trained and fine-tuned model for the same image, to preserve the input-output behaviour of the pre-trained model.

7 Concluding Remarks

We explored how well-known end-to-end fine-tuning approaches often applied to boost the performance of foundation models on downstream tasks can, in turn, significantly damage the model’s ability to recognize general concepts outside the fine-tuning task at hand, a phenomenon which we call concept forgetting. Such an effect is undesirable particularly for foundation models which have been specifically trained on millions of samples to encode information on a vast number of real-world concepts. We observed that fine-tuning method (L2SP) that keeps a model in the vicinity of the pre-trained model in their parameter space did suffer much less from concept forgetting compared to other baselines. Following the intuitions gained from the analysis of L2SP, we conjectured that perhaps vicinity in the feature space might make more sense as the so-called concepts are encoded there, therefore, proposed a new regularizer (LDIFS) that, while fine-tuning, enforced the features of fine-tuned model to be in the vicinity of the pre-trained ones. Through extensive analysis on 9 different downstream classification tasks, we showed that LDIFS significantly alleviated concept forgetting without impeding the downstream task performance.

Future work Though we investigated concept forgetting during fine-tuning and proposed a fix with promising results, we believe that various other experiments and analyses along these lines would be valuable for the community. For example, while we used a contrastive pre-trained model like CLIP for our analysis, understanding such phenomena in other foundation model families such as Large Language Models for instance, would be interesting. Furthermore, fundamentally defining what a “concept” is and the granularity at which we should study it for foundation models is also important and requires serious research efforts to understand phenomena like “concept forgetting” beyond just performing task-based performance evaluation on some downstream dataset. Additionally, studying continual fine-tuning to encourage knowledge accumulation in foundation models certainly opens new avenues for future work.

Acknowledgements This work is supported by the UKRI grant: Turing AI Fellowship EP/W002981/1 and EPSRC/MURI grant: EP/N019474/1. The authors would also like to thank the Royal Academy of Engineering and FiveAI.

References

- [1] Rishi Bommasani, Drew A Hudson, Ehsan Adeli, Russ Altman, Simran Arora, Sydney von Arx, Michael S Bernstein, Jeannette Bohg, Antoine Bosselut, Emma Brunskill, et al. On the opportunities and risks of foundation models. *arXiv preprint arXiv:2108.07258*, 2021.
- [2] Arslan Chaudhry, Puneet K Dokania, Thalaiyasingam Ajanthan, and Philip HS Torr. Riemannian walk for incremental learning: Understanding forgetting and intransigence. In *Proceedings of the European conference on computer vision (ECCV)*, pages 532–547, 2018.
- [3] Gong Cheng, Junwei Han, and Xiaoqiang Lu. Remote sensing image scene classification: Benchmark and state of the art. *Proceedings of the IEEE*, 105(10):1865–1883, 2017.
- [4] M. Cimpoi, S. Maji, I. Kokkinos, S. Mohamed, , and A. Vedaldi. Describing textures in the wild. In *Proceedings of the IEEE Conf. on Computer Vision and Pattern Recognition (CVPR)*, 2014.
- [5] Peng Gao, Shijie Geng, Renrui Zhang, Teli Ma, Rongyao Fang, Yongfeng Zhang, Hongsheng Li, and Yu Qiao. Clip-adapter: Better vision-language models with feature adapters. *arXiv preprint arXiv:2110.04544*, 2021.
- [6] Jiaxin Ge, Hongyin Luo, Siyuan Qian, Yulu Gan, Jie Fu, and Shanghang Zhan. Chain of thought prompt tuning in vision language models. *arXiv preprint arXiv:2304.07919*, 2023.
- [7] Sachin Goyal, Ananya Kumar, Sankalp Garg, Zico Kolter, and Aditi Raghunathan. Finetune like you pretrain: Improved finetuning of zero-shot vision models. *arXiv preprint arXiv:2212.00638*, 2022.
- [8] Patrick Helber, Benjamin Bischke, Andreas Dengel, and Damian Borth. Eurosat: A novel dataset and deep learning benchmark for land use and land cover classification. *IEEE Journal of Selected Topics in Applied Earth Observations and Remote Sensing*, 2019.
- [9] Gabriel Ilharco, Marco Tulio Ribeiro, Mitchell Wortsman, Suchin Gururangan, Ludwig Schmidt, Hannaneh Hajishirzi, and Ali Farhadi. Editing models with task arithmetic. *arXiv preprint arXiv:2212.04089*, 2022.
- [10] Gabriel Ilharco, Mitchell Wortsman, Samir Yitzhak Gadre, Shuran Song, Hannaneh Hajishirzi, Simon Kornblith, Ali Farhadi, and Ludwig Schmidt. Patching open-vocabulary models by interpolating weights. *arXiv preprint arXiv:2208.05592*, 2022.
- [11] Gabriel Ilharco, Mitchell Wortsman, Ross Wightman, Cade Gordon, Nicholas Carlini, Rohan Taori, Achal Dave, Vaishaal Shankar, Hongseok Namkoong, John Miller, Hannaneh Hajishirzi, Ali Farhadi, and Ludwig Schmidt. Openclip, jul 2021.
- [12] Chao Jia, Yinfei Yang, Ye Xia, Yi-Ting Chen, Zarana Parekh, Hieu Pham, Quoc Le, Yun-Hsuan Sung, Zhen Li, and Tom Duerig. Scaling up visual and vision-language representation learning with noisy text supervision. In *International Conference on Machine Learning*, pages 4904–4916. PMLR, 2021.

- [13] Ronald Kemker, Marc McClure, Angelina Abitino, Tyler Hayes, and Christopher Kanan. Measuring catastrophic forgetting in neural networks. In *Proceedings of the AAAI conference on artificial intelligence*, volume 32, 2018.
- [14] James Kirkpatrick, Razvan Pascanu, Neil Rabinowitz, Joel Veness, Guillaume Desjardins, Andrei A Rusu, Kieran Milan, John Quan, Tiago Ramalho, Agnieszka Grabska-Barwinska, et al. Overcoming catastrophic forgetting in neural networks. *Proceedings of the national academy of sciences*, 114(13):3521–3526, 2017.
- [15] Jonathan Krause, Michael Stark, Jia Deng, and Li Fei-Fei. 3d object representations for fine-grained categorization. In *Proceedings of the IEEE international conference on computer vision workshops*, pages 554–561, 2013.
- [16] Alex Krizhevsky, Geoffrey Hinton, et al. Learning multiple layers of features from tiny images. 2009.
- [17] Ananya Kumar, Aditi Raghunathan, Robbie Jones, Tengyu Ma, and Percy Liang. Fine-tuning can distort pretrained features and underperform out-of-distribution. *arXiv preprint arXiv:2202.10054*, 2022.
- [18] Yann LeCun, Léon Bottou, Yoshua Bengio, and Patrick Haffner. Gradient-based learning applied to document recognition. *Proceedings of the IEEE*, 86(11):2278–2324, 1998.
- [19] David Lopez-Paz and Marc’Aurelio Ranzato. Gradient episodic memory for continual learning. *Advances in neural information processing systems*, 30, 2017.
- [20] Ilya Loshchilov and Frank Hutter. Decoupled weight decay regularization. *arXiv preprint arXiv:1711.05101*, 2017.
- [21] Michael McCloskey and Neal J Cohen. Catastrophic interference in connectionist networks: The sequential learning problem. In *Psychology of learning and motivation*, volume 24, pages 109–165. Elsevier, 1989.
- [22] Yuval Netzer, Tao Wang, Adam Coates, Alessandro Bissacco, Bo Wu, and Andrew Y Ng. Reading digits in natural images with unsupervised feature learning. 2011.
- [23] OpenAI. Chatgpt: An ai language model by openai. <https://openai.com>, 2020.
- [24] Omiros Pantazis, Gabriel Brostow, Kate Jones, and Oisín Mac Aodha. Svl-adapter: Self-supervised adapter for vision-language pretrained models. *arXiv preprint arXiv:2210.03794*, 2022.
- [25] F. Pedregosa, G. Varoquaux, A. Gramfort, V. Michel, B. Thirion, O. Grisel, M. Blondel, P. Prettenhofer, R. Weiss, V. Dubourg, J. Vanderplas, A. Passos, D. Cournapeau, M. Brucher, M. Perrot, and E. Duchesnay. Scikit-learn: Machine learning in Python. *Journal of Machine Learning Research*, 12:2825–2830, 2011.
- [26] Alec Radford, Jong Wook Kim, Chris Hallacy, Aditya Ramesh, Gabriel Goh, Sandhini Agarwal, Girish Sastry, Amanda Askell, Pamela Mishkin, Jack Clark, et al. Learning transferable visual models from natural language supervision. In *International conference on machine learning*, pages 8748–8763. PMLR, 2021.
- [27] Sylvestre-Alvise Rebuffi, Alexander Kolesnikov, Georg Sperl, and Christoph H Lampert. icarl: Incremental classifier and representation learning. In *Proceedings of the IEEE conference on Computer Vision and Pattern Recognition*, pages 2001–2010, 2017.
- [28] Manli Shu, Weili Nie, De-An Huang, Zhiding Yu, Tom Goldstein, Anima Anandkumar, and Chaowei Xiao. Test-time prompt tuning for zero-shot generalization in vision-language models. *arXiv preprint arXiv:2209.07511*, 2022.
- [29] Johannes Stalldkamp, Marc Schlipf, Jan Salmen, and Christian Igel. Man vs. computer: Benchmarking machine learning algorithms for traffic sign recognition. *Neural networks*, 32:323–332, 2012.

- [30] Jingchen Sun, Jiayu Qin, Zihao Lin, and Changyou Chen. Prompt tuning based adapter for vision-language model adaption. *arXiv preprint arXiv:2303.15234*, 2023.
- [31] Mitchell Wortsman, Gabriel Ilharco, Samir Ya Gadre, Rebecca Roelofs, Raphael Gontijo-Lopes, Ari S Morcos, Hongseok Namkoong, Ali Farhadi, Yair Carmon, Simon Kornblith, and Ludwig Schmidt. Model soups: averaging weights of multiple fine-tuned models improves accuracy without increasing inference time. In Kamalika Chaudhuri, Stefanie Jegelka, Le Song, Csaba Szepesvari, Gang Niu, and Sivan Sabato, editors, *Proceedings of the 39th International Conference on Machine Learning*, volume 162 of *Proceedings of Machine Learning Research*, pages 23965–23998. PMLR, 17–23 Jul 2022.
- [32] Mitchell Wortsman, Gabriel Ilharco, Jong Wook Kim, Mike Li, Simon Kornblith, Rebecca Roelofs, Raphael Gontijo Lopes, Hannaneh Hajishirzi, Ali Farhadi, Hongseok Namkoong, et al. Robust fine-tuning of zero-shot models. In *Proceedings of the IEEE/CVF Conference on Computer Vision and Pattern Recognition*, pages 7959–7971, 2022.
- [33] LI Xuhong, Yves Grandvalet, and Franck Davoine. Explicit inductive bias for transfer learning with convolutional networks. In *International Conference on Machine Learning*, pages 2825–2834. PMLR, 2018.
- [34] Jiahui Yu, Zirui Wang, Vijay Vasudevan, Legg Yeung, Mojtaba Seyedhosseini, and Yonghui Wu. Coca: Contrastive captioners are image-text foundation models. *arXiv preprint arXiv:2205.01917*, 2022.
- [35] Renrui Zhang, Rongyao Fang, Wei Zhang, Peng Gao, Kunchang Li, Jifeng Dai, Yu Qiao, and Hongsheng Li. Tip-adapter: Training-free clip-adapter for better vision-language modeling. *arXiv preprint arXiv:2111.03930*, 2021.
- [36] Richard Zhang, Phillip Isola, Alexei A Efros, Eli Shechtman, and Oliver Wang. The unreasonable effectiveness of deep features as a perceptual metric. In *Proceedings of the IEEE conference on computer vision and pattern recognition*, pages 586–595, 2018.
- [37] Kaiyang Zhou, Jingkang Yang, Chen Change Loy, and Ziwei Liu. Conditional prompt learning for vision-language models. In *Proceedings of the IEEE/CVF Conference on Computer Vision and Pattern Recognition*, pages 16816–16825, 2022.
- [38] Kaiyang Zhou, Jingkang Yang, Chen Change Loy, and Ziwei Liu. Learning to prompt for vision-language models. *International Journal of Computer Vision*, 130(9):2337–2348, 2022.

In Appendix A, we provide training details for each of our fine-tuning run. In Appendix B, we provide details on how to compute the concatenated feature vector $\Phi_\theta(\mathbf{x})$ from a ViT-B/32 CLIP model for LDIFS. In Appendix C, we provide additional results on **i**) observing how fine-tuning can lead to concept forgetting, **ii**) our investigations on why LP-init-L2SP is a better baseline compared to others in avoiding concept forgetting and **iii**) performance of our proposed LDIFS regularizer.

A Training details

Training datasets and hyper-parameters: We fine-tune the CLIP ViT-B/32 model on each of the 9 image classification datasets: **a**) Stanford Cars, **b**) CIFAR-10, **c**) CIFAR-100, **d**) DTD, **e**) EuroSAT, **f**) GTSRB, **g**) MNIST, **h**) RESISC45, **i**) SVHN. For each dataset, we have a separate fine-tune run for each of the baselines discussed in §2. For each run, we train using the AdamW [20] optimizer, with an initial learning rate of $1e-5$, a weight decay of 0.1 and a cosine learning rate scheduler with a warmup length of 500. For all the runs, we use a batch-size of 128. Following the code of [9], we use the following number of epochs to fine-tune each dataset: **a**) Stanford Cars: 35 epochs, **b**) CIFAR-10/100: 10 epochs, **c**) DTD: 76 epochs, **d**) EuroSAT: 12 epochs, **e**) GTSRB: 11 epochs, **f**) MNIST: 10 epochs, **g**) RESISC45: 15 epochs and **h**) SVHN: 10 epochs. For each dataset, we keep a minimum of 10 epochs for fine-tuning.

Compute and number of experiments: Each of our fine-tuning run is done on a single NVIDIA A100 GPU. As there are a total of 9 classification datasets and a 8 fine-tuning baselines (including our proposed LDIFS), we perform a total of 72 fine-tune training runs from a pre-trained CLIP ViT-B/32. Furthermore, in order to produce the plots capturing \mathcal{A}_{ZS} , \mathcal{A}_{LP} , as well as ℓ_2 distance in parameter and feature space, we store intermediate checkpoints over the course of fine-tuning. Particularly, for each run, we evaluate checkpoints after every 20% of training completion. Finally, in order to obtain the full set of results in Table 3, for the 72 fine-tuned models, we evaluate each of them on 9 datasets (i.e., including the test set of the fine-tuned task), thereby having a total of 648 evaluations. Similar to training, each evaluation is also performed on a single NVIDIA A100 GPU.

B Computing $\Phi_\theta(\mathbf{x})$

In this section, we discuss how we compute the concatenated feature vector $\Phi_\theta(\mathbf{x})$ given input \mathbf{x} and model parameters θ , specifically for a ViT-B/32 model. This is used for computing LDIFS, our proposed regularizer for fine-tuning.

Let the feature output from layer l in the network for input \mathbf{x} be $\Phi_{\theta(l)}(\mathbf{x}) \in \mathbb{R}^l$. Then the normalized feature vector for layer l can be represented as $\frac{\Phi_{\theta(l)}(\mathbf{x})}{\|\Phi_{\theta(l)}(\mathbf{x})\|}$. In order to form the concatenated feature vector, one can technically take features from every intermediate layer of the network. However, storing all the features is memory intensive. Thus, we follow a similar approach to the LPIPS [36] implementation for VGG and AlexNet, and choose 5 intermediate points in the ViT-B/32 architecture to collect features from. For a single input image $\mathbf{x} \in \mathbb{R}^{3 \times 224 \times 224}$, each of the intermediate feature representations has a dimension of $\mathbb{R}^{50 \times 768}$ with 50 tokens and 768 dimensional representation for each token. When normalizing the feature vector, we flatten this vector out to a single 38400 dimensional vector. Thus the full concatenated feature vector $\Phi_\theta(\mathbf{x})$ has dimensionality $5 \times 38400 = 192000$. However, note that there can be other ablations to this design and we leave that for future exploration.

C Additional results

In this section, we present additional empirical results to supplement our observations and conclusions in the main paper.

C.1 Crippling effect of fine-tuning

In §3, we observed how most existing fine-tuning methods, while gaining state-of-the-art performance on fine-tuned tasks, can lead to concept forgetting in models. In this section, we provide additional empirical results to further strengthen those observations.

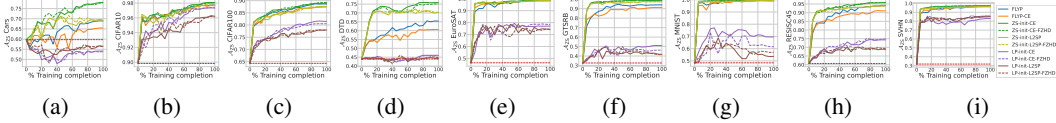


Figure 7: **Test set ZS Accuracy \mathcal{A}_{ZS} for different fine-tuning methods** on 9 image classification tasks: (a) Stanford Cars, (b) CIFAR-10, (c) CIFAR-100, (d) DTD, (e) EuroSAT, (f) GTSRB, (g) MNIST (h) RESISC45 and (i) SVHN. \mathcal{A}_{ZS} generally rises over the course of fine-tuning. However, for the ZS-init-L2SP and LP-init-L2SP baselines, the gain in \mathcal{A}_{ZS} is relatively lower. Furthermore, for LP-init baselines, the performance is consistently lower compared to other baselines

In Figure 7 and Figure 11, we present the \mathcal{A}_{ZS} and \mathcal{A}_{LP} accuracy for models fine-tuned on each of the 9 classification tasks, on their respective test sets. This shows expected behaviour as models broadly achieve very high test set accuracy, which increases over the course of fine-tuning, on their respective fine-tuned tasks. Note that LP-init baselines seem to have relatively lower performance on \mathcal{A}_{ZS} accuracy compared to their ZS-init counter-parts. However, this reduced performance is only limited to \mathcal{A}_{ZS} as this does not translate to a reduced performance in \mathcal{A}_{LP} . Moreover, L2SP baselines (both ZS and LP-init) obtain relatively lower fine-tuned accuracy both in case of \mathcal{A}_{ZS} and \mathcal{A}_{LP} .

In Figure 8 and Figure 12, we present the \mathcal{A}_{ZS} and \mathcal{A}_{LP} for models fine-tuned on EuroSAT (first row), GTSRB (second row) and SVHN (third row) as captured on 8 classification datasets different from their respective fine-tuned set. Broadly, the ZS and LP performance for all models drops on other datasets as they are fine-tuned, thereby capturing concept forgetting in the fine-tuned models. Among the baselines, we consistently observe LP-init-L2SP to perform better than others in avoiding concept forgetting. This is evident through the distinctly higher \mathcal{A}_{ZS} and \mathcal{A}_{LP} accuracies over fine-tuning for the LP-init-L2SP baselines.

C.2 Analysing L2SP

In this section, we provide additional results to supplement our observations related to investigating the L2SP baseline in §4 of the main paper. In Figure 15, we present the ℓ_2 distance in parameter space $\|\theta - \theta_0\|_2^2$ between the pre-trained and current models captured over fine-tuning. For all the datasets, we observe that L2SP baselines while initially diverging slightly in the parameter space, converge back to a model having low ℓ_2 parameter space distance from the original foundation model. Other baselines on the other hand, completely diverge away from the original model in the parameter space.

To further investigate the change in input-output behaviour of the model over fine-tuning, we measure the distance in feature space (see Equation (3)) over fine-tuning. In Figure 16, we present the ℓ_2 distance in feature space captured for models fine-tuned on EuroSAT. Again, consistent with our previous observation, we find that unlike other baselines, L2SP first diverges away from the original foundation model and then converges back to the original input-output behaviour, as is indicative through a decreasing L2 feature space distance in the later stages of fine-tuning. This observation is consistent on the EuroSAT train set, the EuroSAT test set as well as on other datasets, thereby providing our motivation for the LDIFS regularizer.

C.3 Performance of LDIFS

In this section, we provide additional results to supplement observations related to the performance of the proposed LDIFS regularizer.

Choosing λ_{LDIFS} : One hyper-parameter which the LDIFS regularizer introduces is λ_{LDIFS} . A higher value of λ_{LDIFS} encourages the model to preserve features of the original foundation model and vice versa. For each classification task, we performed a grid search over $\lambda_{LDIFS} \in \{0.01, 0.05, 0.1, 0.5, 1, 10, 100\}$ and cross-validated this hyper-parameter on a held-out validation set, choosing the value which produces the best performance on the validation set. We found $\lambda_{LDIFS} = 10$ to produce the best performance over datasets in general, so all the results we present in this paper are with λ_{LDIFS} set to 10.

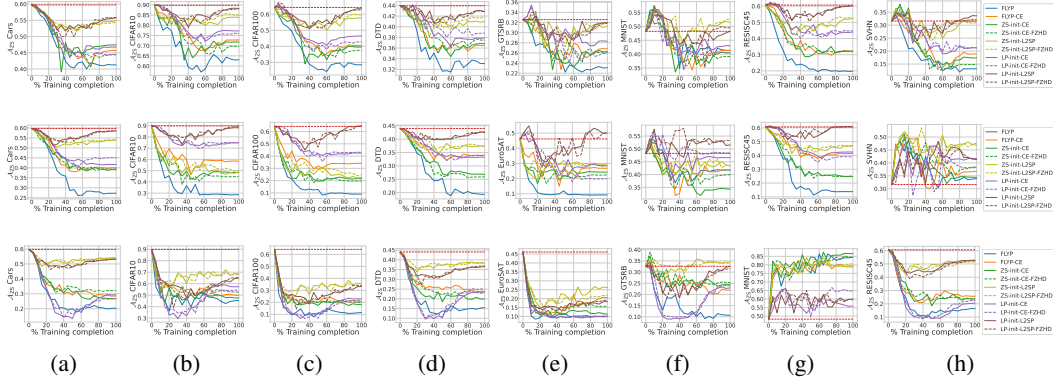


Figure 8: **ZS Accuracy \mathcal{A}_{ZS} for models fine-tuned on EuroSAT (first row), GTSRB (second row), and SVHN (third row) and evaluated on 8 different datasets different from their fine-tuning dataset.** Most fine-tuning methods show a drop in \mathcal{A}_{ZS} performance over the course of fine-tuning indicating a reduction in the model’s transferability.

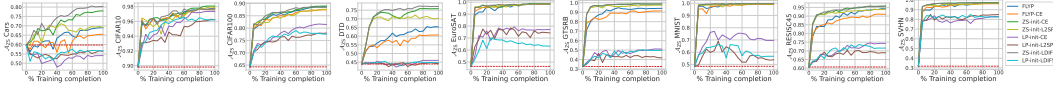


Figure 9: **Comparing test set ZS Accuracy \mathcal{A}_{ZS} for different fine-tuning methods with LDIFS on 9 image classification tasks.** While LP-init baselines generally underperform on \mathcal{A}_{ZS} , we find ZS-init-LDIFS to be competitive with the best baselines.

Results and observations: Firstly, in Figure 9 and Figure 13, we present the test set accuracy of all fine-tuning methods including LDIFS on all 9 classification tasks. We see that LDIFS performs competitively with all other baselines and improves on L2SP consistently. In Figure 10 and Figure 14, we present the \mathcal{A}_{ZS} and \mathcal{A}_{LP} accuracy respectively, for models fine-tuned on EuroSAT (first row), GTSRB (second row) and SVHN (third row) over the course of fine-tuning. Furthermore, we also provide the Δ_{ZS} , Δ_{LP} and the \mathcal{A}_{LP} values for fully fine-tuned models on all 9 classification tasks and all baselines in Table 3.

As is crystal clear from our results, LP-init-LDIFS consistently minimizes concept forgetting without compromising on performance on the fine-tuned task. This is evident from its high \mathcal{A}_{ZS} , \mathcal{A}_{LP} (see Figure 10 and Figure 14) and high Δ_{ZS} and Δ_{LP} (see Table 3) when evaluated on tasks other than the fine-tuning task at hand. Note from Table 3 that even when LP-init-LDIFS is not achieving the best performance on a certain dataset pair, it is often a close second with very little difference compared to the best performing baseline. In addition to this advantage, its \mathcal{A}_{LP} accuracy on the fine-tuned task itself is very competitive with the top scores obtained by other fine-tuning baselines and provides a consistent improvement on L2SP.

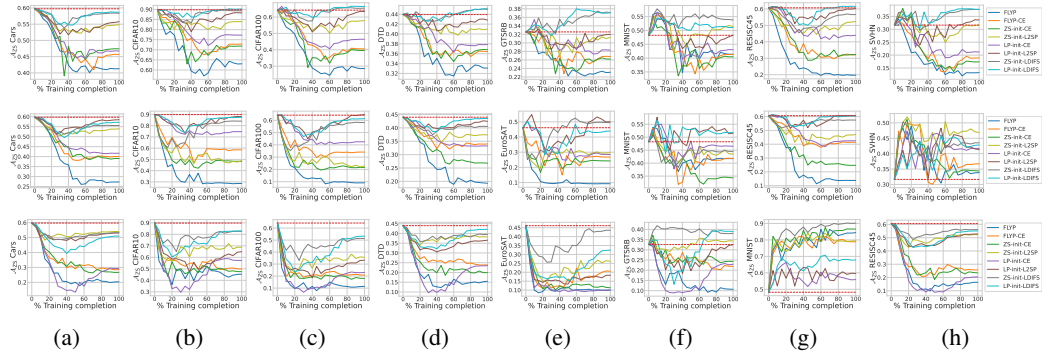


Figure 10: Comparing ZS Accuracy \mathcal{A}_{ZS} of different fine-tuning methods with LDIFS for models fine-tuned on EuroSAT (first row), GTSRB (second row) and SVHN (third row) and evaluated on 8 datasets different from their fine-tuning dataset. LP-init-LDIFS almost consistently beats all other baselines including LP-init-L2SP in preserving the model’s transferability.

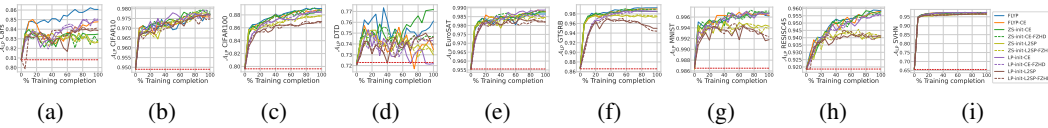


Figure 11: Test set LP Accuracy \mathcal{A}_{LP} for different fine-tuning methods on 9 image classification tasks: (a) Stanford Cars, (b) CIFAR-10, (c) CIFAR-100, (d) DTD, (e) EuroSAT, (f) GTSRB, (g) MNIST (h) RESISC45 and (i) SVHN. \mathcal{A}_{LP} generally rises over the course of fine-tuning. However, for the ZS-init-L2SP and LP-init-L2SP baselines, the gain in \mathcal{A}_{LP} is relatively lower. Furthermore, for LP-init baselines, the performance is consistently lower compared to other baselines

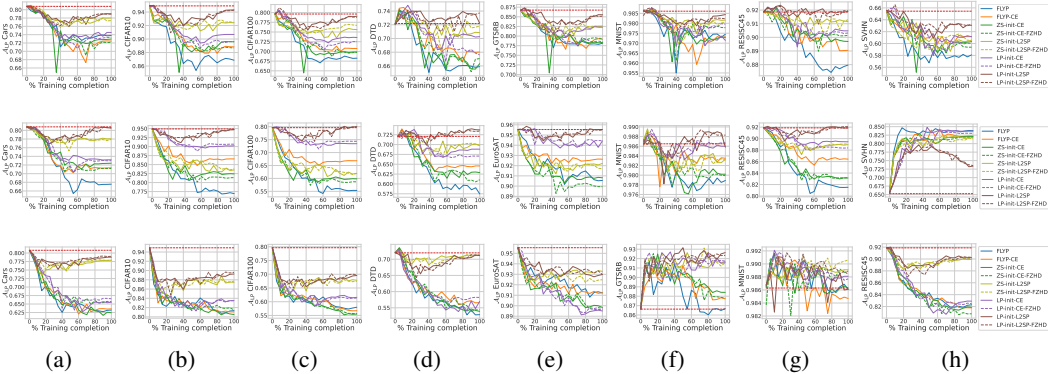


Figure 12: LP Accuracy \mathcal{A}_{LP} for models fine-tuned on EuroSAT (first row), GTSRB (second row), and SVHN (third row) and evaluated on 8 different datasets different from their fine-tuning dataset. Most fine-tuning methods show a drop in \mathcal{A}_{LP} performance over the course of fine-tuning indicating a reduction in the model’s transferability.



Figure 13: Comparing test set LP Accuracy \mathcal{A}_{LP} for different fine-tuning methods with LDIFS on 9 image classification tasks.

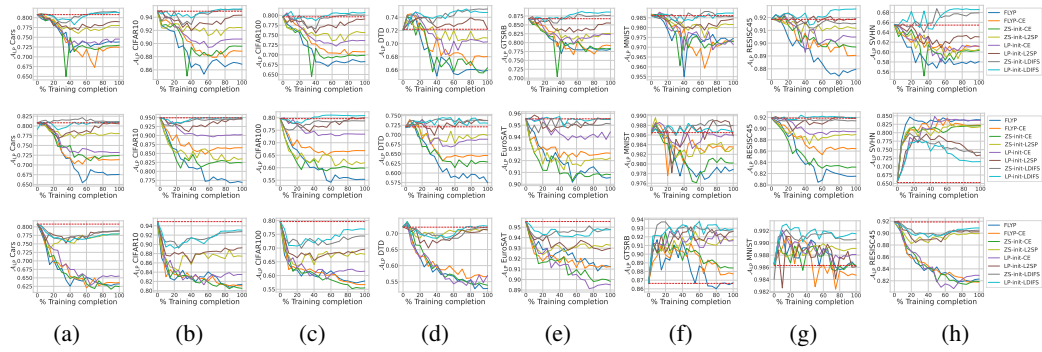


Figure 14: **Comparing LP Accuracy \mathcal{A}_{LP} of different fine-tuning methods with LDIFS for models fine-tuned on EuroSAT (first row), GTSRB (second row) and SVHN (third row) and evaluated on 8 datasets different from their fine-tuning dataset. LP-init-LDIFS almost consistently beats all other baselines including LP-init-L2SP in preserving the model’s transferability.**

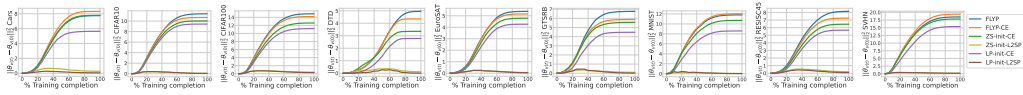


Figure 15: **ℓ_2 distance in weight space $\|\theta - \theta_0\|_2^2$ between pre-trained image encoder f_{θ_0} and fine-tuned image encoder f_{θ} over the course of fine-tuning. Apart from ZS-init-L2SP and LP-init-L2SP, all fine-tuning baselines diverge in weight space over the course of fine-tuning.**

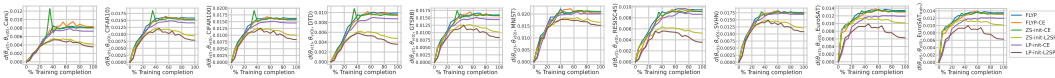


Figure 16: **ℓ_2 distance in feature space $d(\theta, \theta_0, \mathcal{D})$, between fine-tuned and pre-trained image encoders, f_{θ} and f_{θ_0} computed over different fine-tuning methods for models fine-tuned on EuroSAT.**

Dataset	Eval	Fine-tuning baselines																							
		FLP			FLP-CE			ZS-init-CE			LP-init-L2SP			LP-init-L2SP			ZS-init-LDIFS			LP-init-LDIFS (Ours)					
File name		$\Delta_{ZS}(\uparrow)$	$\Delta_{LP}(\uparrow)$	$\Delta_{LP}(\uparrow)$	$\Delta_{ZS}(\uparrow)$	$\Delta_{LP}(\uparrow)$	$\Delta_{LP}(\uparrow)$	$\Delta_{ZS}(\uparrow)$	$\Delta_{LP}(\uparrow)$	$\Delta_{LP}(\uparrow)$	$\Delta_{ZS}(\uparrow)$	$\Delta_{LP}(\uparrow)$	$\Delta_{LP}(\uparrow)$	$\Delta_{ZS}(\uparrow)$	$\Delta_{LP}(\uparrow)$	$\Delta_{LP}(\uparrow)$	$\Delta_{ZS}(\uparrow)$	$\Delta_{LP}(\uparrow)$	$\Delta_{LP}(\uparrow)$	$\Delta_{ZS}(\uparrow)$	$\Delta_{LP}(\uparrow)$	$\Delta_{LP}(\uparrow)$			
Can	CFAR10	-3.55	-0.68	94.24	-9.0	-1.74	93.18	-9.81	-1.52	93.4	-10.42	-0.93	94.0	-2.78	-0.89	94.02	-0.26	0.06	94.97	-2.98	-0.47	94.45	-2.85	-0.22	94.69
	CFAR100	-6.91	-0.76	78.89	-7.41	-2.74	76.91	-8.62	-3.58	76.04	-6.84	-2.12	77.51	-3.4	-2.28	77.34	0.22	0.17	79.81	-1.6	-0.37	79.26	-1.76	0.07	79.71
	FDI	-2.61	1.28	73.46	-4.2	-1.44	70.9	-3.99	0.53	72.5	-3.99	2.13	74.26	-3.09	-0.64	71.44	-1.17	2.39	74.63	-1.54	-0.32	71.76	-2.34	0.43	72.55
	EuroSAT	-16.94	-0.2	95.33	-5.89	-0.54	95.0	-6.09	-0.8	94.74	2.74	-0.02	95.52	-1.8	-0.56	94.08	-2.46	0.02	95.66	1.0	-0.13	95.41	4.41	0.02	95.66
	GTSRB	-3.62	0.55	87.49	-4.28	-1.39	85.24	-1.1	-0.66	85.96	-3.58	-1.01	85.62	2.19	-0.4	86.21	1.85	0.64	87.21	2.36	-0.02	86.56	0.74	0.44	87.18
	MNIST	4.28	-0.19	98.56	2.26	-0.52	98.31	4.29	-0.43	98.48	2.21	-0.14	98.48	1.46	-0.34	98.33	2.45	-0.07	98.59	2.33	0.01	98.71	2.15	0.06	98.62
	RESISC45	0.33	1.14	96.62	-5.4	-3.39	92.35	-1.63	-3.91	91.47	-0.7	-2.09	93.49	2.92	-2.01	93.51	1.54	0.78	96.08	-0.95	-1.33	95.51	1.93	0.53	96.01
SVHN	9.2	1.21	90.67	-7.16	-1.07	90.3	-10.7	-2.13	89.75	-4.81	-0.87	91.0	-4.48	-1.4	90.48	-0.21	-0.25	91.62	-4.13	-0.48	91.4	-2.7	-0.13	91.75	
SVHN	0.33	1.14	96.62	-5.4	-3.39	92.35	-1.63	-3.91	91.47	-0.7	-2.09	93.49	2.92	-2.01	93.51	1.54	0.78	96.08	-0.95	-1.33	95.51	1.93	0.53	96.01	
Can	5.2	6.25	86.06	5.73	3.95	84.77	18.24	2.67	83.48	-5.62	4.14	84.95	9.44	1.83	82.64	-3.31	3.06	83.87	20.52	4.71	85.52	-3.15	4.45	85.96	
CFAR10	Can	-58.0	-14.58	66.24	-45.32	-7.04	78.75	-46.08	-5.68	75.12	-36.86	-8.27	72.53	-15.81	0.52	81.32	-4.19	-0.55	80.26	-13.78	0.53	81.33	-8.95	-1.31	79.51
	CFAR100	-19.22	0.97	89.62	-0.33	1.86	81.52	-2.39	1.86	81.02	0.23	2.85	82.46	8.79	4.81	84.45	8.97	5.22	84.85	3.08	0.28	79.32	3.1	2.12	81.74
	FDI	-14.31	-7.63	64.15	-9.52	-4.52	67.71	-9.73	-6.06	66.01	-9.52	-4.36	67.77	-1.86	1.38	78.46	-2.77	-0.74	71.33	-0.8	0.27	72.34	-0.69	0.05	72.18
	EuroSAT	-16.93	-0.07	95.46	-14.76	-0.3	95.24	-18.06	-0.19	95.35	-17.04	-0.33	95.2	4.2	-0.07	95.46	-1.09	0.44	95.98	0.17	0.07	96.01	2.83	0.46	96.0
	GTSRB	-2.72	-1.24	85.3	-0.45	87.65	-2.16	-0.48	86.25	-0.33	1.03	87.7	1.63	1.15	87.82	-0.87	1.58	88.23	5.81	2.84	89.05	5.38	2.31	89.69	
	MNIST	-9.31	-0.45	98.23	-10.42	-0.07	98.59	-12.21	-0.1	98.54	-4.02	0.22	98.73	2.4	-0.1	98.55	2.25	-0.13	98.52	-0.4	0.91	98.62	0.21	-0.17	98.69
	RESISC45	-26.32	-4.83	87.65	-14.44	-2.54	89.33	-13.49	-2.51	89.37	-16.32	-1.97	90.9	-0.29	-0.25	91.62	-1.49	-0.1	91.78	0.25	0.17	92.05	1.03	0.13	92.0
SVHN	-3.49	1.36	66.84	-7.19	2.9	68.33	-5.45	0.4	65.98	0.62	4.34	69.95	7.15	3.71	69.22	7.08	3.59	69.13	6.17	3.97	69.34	8.13	4.92	70.4	
CFAR10	7.87	2.79	97.71	7.8	2.65	97.58	8.25	2.83	97.71	7.5	2.79	97.71	8.05	2.8	97.7	6.38	2.74	97.66	7.72	2.46	97.96	6.39	2.33	97.24	
CFAR100	Can	-27.76	-3.15	77.66	-12.67	-3.36	77.44	-21.22	-3.58	77.23	-12.42	-4.38	76.42	-6.74	-0.12	80.69	1.32	0.15	80.96	-12.29	-0.72	80.08	-6.32	-1.07	79.73
	CFAR100	-8.17	1.05	95.96	0.22	1.33	96.26	-0.64	1.5	96.41	1.06	1.22	96.42	2.65	1.96	96.87	3.24	1.62	96.51	0.33	1.34	96.25	0.41	0.88	95.79
	FDI	-10.37	-6.41	65.64	-8.83	-5.53	66.54	-9.36	-5.11	66.97	-6.54	-3.3	68.83	-4.52	-0.74	71.33	-2.39	0.16	72.23	-4.41	-1.44	70.64	-1.97	-1.37	70.71
	EuroSAT	-23.19	-0.86	95.48	-12.86	-0.26	95.28	-16.59	-0.48	95.06	-7.11	-0.17	95.37	-6.46	0.19	95.72	-7.13	0.46	96.0	-3.33	0.28	95.8	-2.19	0.66	96.09
	GTSRB	-6.46	0.17	86.79	-0.43	2.52	89.11	-4.64	0.99	87.62	2.98	2.69	89.2	1.27	1.8	88.42	3.2	2.65	89.18	4.88	2.98	89.05	6.08	4.04	90.07
	MNIST	-8.99	-0.35	98.36	-7.26	-0.15	98.51	-1.37	-0.3	98.36	-0.36	0.11	98.79	3.09	0.08	98.52	2.85	0.04	98.75	8.11	-0.07	98.68	0.25	0.2	98.04
	RESISC45	-20.65	-3.54	88.33	-16.51	-3.36	88.32	-17.65	-3.3	88.57	-14.14	-1.95	89.92	-5.78	-1.3	90.59	-2.81	-0.37	91.3	-7.68	-1.1	90.78	-5.49	-0.44	91.43
SVHN	2.46	3.08	68.59	6.05	0.04	70.28	2.43	2.27	68.03	4.7	4.64	70.38	7.99	3.3	68.84	6.98	3.7	69.32	6.02	6.32	70.67	8.24	4.68	70.21	
CFAR100	24.4	9.34	88.98	23.16	9.12	88.77	24.63	8.97	88.6	17.26	8.78	88.41	23.33	8.2	87.84	13.77	7.31	86.94	24.24	8.31	87.94	13.3	9.35	88.99	
DTD	Can	-18.69	-3.36	77.44	-10.19	-2.87	77.94	-9.85	-2.54	78.25	-5.97	-2.43	78.36	-11.63	-4.15	76.66	-0.06	0.21	81.01	-1.94	0.77	81.58	-1.32	0.36	81.17
	CFAR10	-36.34	-6.25	88.37	-13.28	-4.32	90.59	-13.4	-4.74	90.17	-9.33	-1.81	93.11	-12.64	-4.99	89.92	4.87	-0.44	94.48	-0.76	-0.22	94.17	0.4	0.21	95.12
	CFAR100	-36.48	-10.03	69.61	-18.82	-7.08	72.67	-20.99	-8.23	71.41	-8.12	-3.3	76.94	-17.73	-8.45	71.18	2.89	0.68	80.45	-3.41	-0.72	78.33	1.61	0.84	80.49
	EuroSAT	-32.07	-10.57	94.96	-20.46	-1.54	94.0	-12.56	-0.48	95.06	-11.02	-0.52	95.02	-22.26	-1.33	94.2	4.87	0.15	95.69	-7.19	0.43	95.96	2.76	0	95.54
	GTSRB	-18.13	-7.62	79.69	-7.89	-3.52	83.13	-13.89	-2.21	84.51	-4.41	-1.61	85.91	-3.76	-2.62	83.97	0.34	-0.39	86.18	2.11	1.8	87.32	2.1	0.11	87.83
	MNIST	-24.64	-0.95	97.75	-3.59	-0.51	98.16	-7.74	0.02	98.35	-5.74	-0.32	98.34	-7.92	-0.14	98.49	6.03	-0.02	98.69	-2.84	0.17	98.86	2.6	0.15	98.84
	RESISC45	-34.51	-5.9	86.87	-11.9	-2.52	90.37	-11.37	-2.65	89.22	-10.52	-1.48	90.4	-19.27	-4.48	87.38	0.34	-0.13	91.75	-1.86	0.28	91.12	1.21	0.14	92.02
SVHN	-17.89	-5.9	59.64	-8.6	-5.14	60.18	-3.31	-3.28	62.14	-3.49	-2.61	63.03	0.55	-3.54	61.9	1.84	-0.11	65.3	7.88	0.36	66.31	3.81	1.23	66.69	
EuroSAT	Can	-18.44	-7.9	72.8	-14.64	-8.34	72.48	-12.84	-7.8	72.95	-13.9	-6.27	73.44	-10.9	-2.79	78.01	-3.85	-1.84	78.97	-3.27	0.43	81.27	-2.18	0.88	81.33
	CFAR10	-21.44	4.04	76.12	-16.7	1.33	75.46	-31.91	4.89	77.18	2.13	0.05	77.18	26.38	0.9	72.98	0.16	2.45	74.63	33.14	6.12	78.14	0.74	3.19	75.27
	CFAR100	-28.75	-6.01	86.86	-17.0	-6.07	88.84	-17.99	-5.32	89.58	-12.57	-4.24	90.68	-5.87	-2.49	92.41	-1.59	-0.4	94.31	-0.53	0.23	93.13	0.39	0.34	95.25
	EuroSAT	-28.88	-11.37	68.26	-23.88	-8.47	69.38	-24.64	-8.47	69.38	-17.79	-2.03	73.89	-24.41	-4.49	75.42	-4.08	-0.56	79.08	-3.23	0.68	80.09	2.27	1.06	80.7
	GTSRB	-9.49	-8.53	78.14	-5.78	-7.54	79.16	-6.39	-8.39	78.35	-4.29	-4.35	82.31	-1.27	-4.05	82.65	-0.58	-1.2	85.53	4.66	0.94	87.67	4.51	1.58	88.76
	MNIST	-6.85	-1.2	97.45	-6.92	-1.35	97.82	-7.76	-1.32	97.29	-5.24	-1.48	97.14	3.21	-0.54	98.16	0.84	-0.2	98.44	5.54	-0.07	98.37	2.82	1.18	98.74
	RESISC45	-40.35	-3.89	87.07	-28.6	-2.83	89.05	-28.44	-2.16	89.7	-16.65	-1.4	90.48	-8.29	-0.7	91.16	-0.46	0.05	91.3	-3.08	-0.33	91.54	0.9	0.79	92.27
SVHN	-18.4																								